

Extending a potential vorticity transport eddy closure to include a spatially-varying coefficient



Qingshan Chen^{a,*}, Todd Ringler^b, Peter R. Gent^c

^a Department of Mathematical Sciences, Clemson University, Clemson, SC 29634, United States

^b Los Alamos National Laboratory, Los Alamos, NM 87501, United States

^c National Center for Atmospheric Research, Boulder, CO 80307, United States

ARTICLE INFO

Article history:

Available online 18 January 2016

Dedicated to the 70th birthday of Max Gunzburger

Keywords:

Antarctic Circumpolar Current
Mesoscale eddy parametrization
Gent–McWilliams closure
Potential vorticity homogenization
Spatially-varying diffusivities

ABSTRACT

The use of spatially varying eddy diffusivities is explored with the extended Gent–McWilliams (eGM) closure for both passive tracers and potential vorticity (PV). Numerical experiments are conducted with a wind-forced isopycnal channel model. It is shown that, the eGM closure with eddy diffusivities derived from a high-resolution reference solution produces the best results compared to the reference solution in terms of the thickness, PV profiles and volume fluxes. The use of spatially varying eddy diffusivities also removes the unphysical reverse jets near the channel walls shown by the eGM with constant eddy diffusivities.

© 2016 Elsevier Ltd. All rights reserved.

1. Introduction

The Gent–McWilliams (GM, Gent and McWilliams [1]; Gent et al. [2]; Gent [3]) closure is an essential component of non-eddy-resolving global ocean models used to study climate. GM serves as a surrogate for the baroclinic instability that is largely responsible for the existence of mesoscale eddies which, in turn, transport a substantial amount of heat polewards. The closure is based on the fundamental assumption that the eddy transport should be down the thickness gradient, and along, not across, isopycnal surfaces. GM is used in conjunction with mixing along isopycnal surfaces that was formalized by Redi [4]. While the closure has seen widespread success in ocean modeling since its introduction (see e.g. [5,6] among many others), there are also aspects of the closure that suggest improvements are possible. For example, in many implementations of GM (exceptions will be discussed below), the closure depends on two parameters, the thickness diffusivity and the isopycnal diffusivity, which are frequently taken as constants in the horizontal and vertical directions. It is natural to ask whether spatially varying parameters are more appropriate.

Many efforts have been made to determine and implement spatially-varying GM parameters. One of the first was Visbeck et al. [7] who proposed that the closure parameter is proportional to the square of the width of the baroclinic zone divided by the time scale determined from the Coriolis parameter and the local Richardson number. There are too many proposals to provide a complete list here. However, very recently Farneti and Gent [8] use the GFDL CM2.1 climate model to test a spatially varying formulation of the eddy-induced advection parameter that is proportional to the vertical average of the horizontal gradients of the potential density field. Hofmann and Morales Maqueda [9] test a formulation close to that of Visbeck et al. [7] in a global ocean model. Both Farneti and Gent [8] and Hofmann and Morales Maqueda [9] confirm that a

* Corresponding author. Tel.: +1 864 656 4565.
E-mail address: qsc@clemson.edu (Q. Chen).

spatially varying formulation of the eddy diffusivity parameter helps to reproduce the insensitivity of the Southern Ocean circulation to strongly intensified Southern Hemisphere westerlies seen in eddy-resolving models.

There is also a long history suggesting the parametrization of mesoscale eddy transport should be based on mixing of the potential vorticity (PV) field, due to its tracer like property; e.g. [10–15]. Ringler and Gent [16] extend the standard GM closure to the momentum equations utilizing the similarity between the PV equation and the equation for a tracer. Energetic analysis shows that, in an adiabatic system with the extended GM closure, the total energy is conserved up to a small error proportional to the temporal changing rate of the bolus velocity (see Eq. (17) therein). The last point is essential because it implies that the extended GM closure preserves the conversion between the available potential energy (APE) and the kinetic energy (KE), up to a small error term. It is well known that the standard GM closure provides a monotone APE sink. The extended GM closure is evaluated in a three-layer isopycnal model for the Antarctic Circumpolar Current (ACC). The standard GM (labeled GMST therein), the extended GM (labeled GMPV therein), together with the standard GM closure with the eddy induced PV transport only (labeled PVBL therein) are applied in the 62.5 km low resolution simulations, and the results are compared to the 10 km reference solution. The performance of the various eddy closures is evaluated in terms of the time mean and zonal mean of the zonal jet velocity and of the PV. The authors come to the conclusion that the extended GM configured with a small eddy mixing coefficient (250 m²/s) is marginally better than the other configurations. However, the extended GM simulations show strong westward currents along the southern and northern boundaries that do not appear in the high-resolution simulation. The authors conjecture that using spatially varying eddy diffusivities that, in particular, vanish near the boundaries can remedy this deficiency for the closure. A much broader question, which is implicit but left un-explored in [16], is whether using spatially varying eddy diffusivity has any merit in simulating the world ocean.

The goals of this work are two-fold. The first is to test the hypothesis made in [16], namely that using spatially varying eddy diffusivities can remedy the deficiency of the extended GM closure mentioned above. For this study, we derive the spatial distribution of the eddy diffusivity using a high-resolution, eddy resolving simulation. Second, in a general setting, we want to answer the question whether using spatially varying eddy diffusivities can improve overall the results of model simulations that do not permit mesoscale eddies. We approach these questions with a set of controlled simulations using a three-layer isopycnal model for the ACC. A 10 km simulation of the model will provide the reference solution for this study. The goal of any subgrid parametrization is to replicate certain features of a high resolution simulation in a low resolution setting. For the latter, we use a 125 km mesh so that the mesoscale eddies are not resolved. In the current study, we do not develop or test any premises on the formulation of the eddy diffusivity. Instead, we use the high resolution data to derive the point-wise eddy diffusivities for each layer, and then feed the derived parameters into the low resolution simulations. We note that a similar approach has been taken in [15], also in a channel domain, although his model is for zonally-averaged quantities and uses a different forcing technique than wind forcing. Care has to be taken with this approach because the parameters derived from the high resolution simulation may have deficiencies (e.g. negative diffusivities) that render the low resolution simulations oscillatory or even unstable.

2. The extended Gent–McWilliams (eGM) closure

A three-layer isopycnal system

For this study, we employ an adiabatic three-layer isopycnal model described by three sets of equations, one for each layer,

$$\begin{cases} \frac{\partial h_i}{\partial t} + \nabla \cdot (h_i \mathbf{u}_i) = 0, \\ \frac{\partial \mathbf{u}_i}{\partial t} + h_i q_i \mathbf{k} \times \mathbf{u}_i = -\nabla \left(\frac{\phi_i}{\rho_0} + K_i \right) + \mathbf{D}_i + \mathbf{F}_i, \\ \frac{\partial}{\partial t} (h_i \sigma_i) + \nabla \cdot (h_i \sigma_i \mathbf{u}_i) = 0, \end{cases} \quad (1)$$

where $i = 1, 2, 3$ is the layer index starting at the ocean surface. The prognostic variables h_i , \mathbf{u}_i and σ_i denote the layer thickness, horizontal velocity, and some tracer respectively, and the diagnostic variables q_i , ϕ_i and K_i denote the potential vorticity, Montgomery potential and kinetic energy, respectively, and they are defined as

$$q_i = \frac{\nabla \times \mathbf{u}_i + f}{h_i}, \quad i = 1, 2, 3,$$

$$K_i = \frac{1}{2} |\mathbf{u}_i|^2, \quad i = 1, 2, 3,$$

$$\phi_1 = p_0 + \rho_1 g (h_1 + h_2 + h_3 + b),$$

$$\phi_2 = \phi_1 + (\rho_2 - \rho_1) g (h_2 + h_3 + b),$$

$$\phi_3 = \phi_2 + (\rho_3 - \rho_2) g (h_3 + b),$$

with p_0 denoting the surface pressure and b the bathymetry; \mathbf{D}_i denotes the horizontal viscous diffusion, which usually takes the form of harmonic or biharmonic diffusion. The external forcing term \mathbf{F}_i for each layer is specified as follows,

$$\mathbf{F}_i = \begin{cases} \frac{\boldsymbol{\tau}}{\rho_1 h_1} \text{ (wind stress),} & i = 1, \\ 0, & i = 2, \\ -\mathbf{d} \text{ (bottom drag),} & i = 3, \end{cases} \quad (2)$$

where $\boldsymbol{\tau}$ is the surface wind stress. This continuous model of the adiabatic ocean isolates both mass and PV into individual layers. The conservative form of (1)(a) clearly shows that mass can be redistributed within a layer via the $\nabla \cdot (h_i \mathbf{u}_i)$ term, but cannot be exchanged between layers. Similarly, if we take the curl of (1)(b) and combine it with (1)(a), the PV equation takes the form

$$\frac{\partial}{\partial t}(h_i q_i) + \nabla \cdot (h_i q_i \mathbf{u}_i) = \nabla \times (\mathbf{D}_i + \mathbf{F}_i). \quad (3)$$

Similar to the continuity equation, the PV transport term can move PV within a layer but cannot exchange PV between the layers. While pressure can act to transfer momentum and energy between layers, the pressure gradient forcing is curl free and, thus, does not transfer vorticity between the layers. The only source/sink of PV in the middle layer is horizontal dissipation that, at least away from the boundary, should act to mix PV. As a result, a homogenized PV field [17] is the only plausible equilibrium state for the middle layer.

In an adiabatic isopycnal system the standard Gent–McWilliams closure modifies the thickness and tracer equations to be

$$\frac{\partial \bar{h}_i}{\partial t} + \nabla \cdot (\bar{h}_i \mathbf{U}_i) = 0, \quad (4)$$

$$\frac{\partial}{\partial t}(\bar{h}_i \bar{\sigma}_i) + \nabla \cdot (\bar{h}_i \bar{\sigma}_i \mathbf{U}_i) = \nabla \cdot (\kappa \bar{h}_i \nabla \bar{\sigma}_i), \quad (5)$$

where \bar{h}_i and $\bar{\sigma}_i$ are the mean (large-scale) thickness and tracer fields averaged over the scales related to mesoscale eddies. The residual transport velocity, \mathbf{U}_i , is defined as the sum of the mean velocity and the bolus velocity,

$$\mathbf{U}_i = \bar{\mathbf{u}}_i + \mathbf{u}_i^*. \quad (6)$$

The GM closure claims that \mathbf{u}_i^* should be down the thickness gradient, i.e.,

$$\mathbf{u}_i^* = -\kappa \frac{\nabla \bar{h}_i}{\bar{h}_i}. \quad (7)$$

In practice, the coefficient κ is very often taken as a global constant, but in the model to be explored below, we will allow κ to vary in space.

Exploiting the similarity between the PV equation and the equation for a passive tracer, Ringler and Gent [16] test an extension to the GM closure (eGM, thereafter) to include a modification to the momentum equation. The modified PV equation takes the form

$$\frac{\partial}{\partial t}(\bar{h}_i \bar{q}_i) + \nabla \cdot (\bar{h}_i \bar{q}_i \mathbf{U}_i) = \nabla \cdot (\kappa \bar{h}_i \nabla \bar{q}_i) + \nabla \times (\mathbf{D}_i + \mathbf{F}_i). \quad (8)$$

In analogy to the RHS of (5), the right-hand side of (8) represents PV mixing due to the mesoscale eddies. The momentum equation consistent with (8) is shown to be

$$\frac{\partial \bar{\mathbf{u}}_i}{\partial t} + (f + \bar{\zeta}_i) \mathbf{k} \times \mathbf{U}_i + \nabla \bar{\phi}_i + \nabla K'_i = \mathbf{k} \times (\kappa \bar{h}_i \nabla \bar{q}_i) + \mathbf{D}_i + \mathbf{F}_i, \quad (9)$$

where $\bar{\zeta}$ is the relative vorticity. This equation demonstrates that the bolus transport of PV can be modeled in the momentum equation by including the bolus velocity in the computation of the nonlinear Coriolis force. In addition, PV mixing is modeled by a skewed PV gradient on the RHS of the momentum equation.

Ringler and Gent [16] show via an energetic analysis that if the kinetic energy K' is defined as

$$K'_i = \frac{1}{2}(\bar{\mathbf{u}}_i \cdot \bar{\mathbf{u}}_i) + (\bar{\mathbf{u}}_i \cdot \mathbf{u}_i^*), \quad (10)$$

then the total energy is conserved up to a small error proportional to $\partial \mathbf{u}_i^* / \partial t$ (see equation (17) of Ringler and Gent [16]). The last point is essential because it implies that the eGM closure preserves the conversion between the available potential energy (APE) and the kinetic energy (KE), up to a small error term. As a result, the flow of energy within the eGM closure better mimics true mesoscale eddies by transferring APE to KE.

Ringler and Gent [16] also discuss in detail the shortcoming of the skewed PV gradient on the RHS of (9). The zonal component of (9) reads

$$\frac{\partial \bar{u}_i}{\partial t} - (f + \bar{\zeta}_i)(\bar{v}_i + v_i^*) + \frac{\partial \bar{\phi}_i}{\partial x} + \frac{\partial K'_i}{\partial x} = -\kappa \bar{h}_i \frac{\partial \bar{q}_i}{\partial y} + D_i + F_i. \tag{11}$$

In large-scale geophysical flows, the PV field is generally dominated by the planetary vorticity field, and therefore, when the flow is at rest with homogeneous layer thickness, the meridional PV gradient in (11) is reduced to $-\kappa \beta \mathbf{i}$, where β is the meridional derivative of planetary vorticity. While such a westward force might be physically correct within regions undergoing PV mixing via mesoscale eddies, it seems untenable to argue for such a force at the largest scales of ocean circulation. In the idealized channel of limited meridional extent, Ringler and Gent [16] found anomalous westward jets near the boundaries outside the region of wind-stress forcing due to the $-\kappa \beta \mathbf{i}$ force. More generally, inclusion of this forcing term in the model raises the issue of non-conservation of momentum [11,15]. Eden [15] proposes the inclusion of a gauge term, which is calculated by balancing the domain integral of the eddy momentum flux. However, it is not clear whether this should be done layer by layer, or just in the integral over all layers. Also, Eden [15] includes a linear viscous term in addition to the eddy forcing, whereas in our model the viscous term is part of the eddy forcing. In this paper, we have chosen not to include a gauge term, but to follow the hypothesis from [16] that κ be allowed to vary spatially. By allowing $\kappa \rightarrow 0$ in regions outside mesoscale mixing, the $-\kappa \beta \mathbf{i}$ force is able to “turn off” in regions where eddies are not present. The primary goal of this paper is to test this hypothesis. We will return to this momentum non-conservation issue in both Sections 3 and 4.

3. GM with spatially-dependent parameters

Model description with 10 km eddy resolving results

The model setup is very similar to that of Ringler and Gent [16], which, in turn, is modeled after the three-layer channel model of McWilliams and Chow [18]. We repeat the details here for reference. The model is configured in a 2000 km × 1732 km domain which is periodic in the zonal direction and bounded by solid walls on the northern and southern boundaries. The β -plane approximation is used with $f_0 = -1.1 \times 10^{-4} \text{ s}^{-1}$ and $\beta = 1.4 \times 10^{-11} \text{ m}^{-1} \text{ s}^{-1}$. The model is made up of three isopycnal layers with mean layer thickness of 500, 1250 and 3250 m and with densities of 1010, 1013 and 1016 kg m⁻³. The system is forced by a zonal wind stress on the top layer with the form $\tau = \tau_0 \exp(-(y - y_0)^2/r^2)$ where $\tau_0 = 0.1 \text{ N m}^{-2}$ and y_0 is the meridional midpoint of the channel and $r = 300 \text{ km}$. This force is balanced by a bottom drag of the form $\mathbf{d} = 10^{-3} \mathbf{u}_3 |\mathbf{u}_3|/h_3$.

The numerical model is based on the Model Prediction Across Scales Ocean model (MPAS-O, Ringler et al. [19,20]). MPAS employs a C-grid finite volume scheme that preserves energy to within time truncation error and the potential vorticity to within machine round-off error.

We use a uniform 10 km hexagonal grid for the high-resolution reference simulation. The usual biharmonic diffusion with a coefficient of $10^9 \text{ m}^4 \text{ s}^{-1}$ is used in the momentum equation, and no other form of diffusion/parametrization is used in the model. For this high-resolution simulation we use a time step $\Delta t = 45 \text{ s}$ with the fourth order Runge–Kutta method, and run the simulation up to 200 years to ensure that an equilibrium state has been reached. Fig. 1 shows snapshots of the PV field around year 200 for all three layers. The top panel shows a meandering jet that is a mixture of turbulent mixing and Rossby wave motions. The color scales for the middle and bottom layers are adjusted to highlight the weak patterns in the PV field in these layers. The largely monochrome interior of the middle layer shows a homogeneous PV field in the interior of the ocean, consistent with Rhines and Young [17]. The bottom panel demonstrates a weak meandering jet and wave-like motion due to the bottom drag.

For the purpose of data analysis, we take 360 samples evenly distributed between year 200 and 210. The zonal-mean of the flow is close to being geostrophically balanced. This can be seen from Fig. 2. On the left panel is the time mean and zonal mean Montgomery potential for each layer, and on the right panel is the time mean zonal mean of the zonal velocity for each layer. The zonal velocities derived from the Montgomery potentials through geostrophic relations differ from the real zonal velocities by a maximum of 18%.

On Fig. 3 are the meridional thickness profiles and the meridional thickness eddy fluxes for all three layers. The top and bottom layers clearly demonstrate downgradient thickness fluxes in the jet region between 600 and 1400 km. The eddy flux of the middle layer is only about one fifth as large as the eddy fluxes of the top/bottom layers. The middle layer demonstrates downgradient thickness fluxes in the half of the jet region closer to the pole and up-gradient thickness fluxes in the other half of the jet region closer to the equator.

The goal of this article is to explore spatially varying coefficients for the GM closure, and we use data from the 10 km high resolution reference simulation as a guide. In a re-entrant channel model the flow, and hence the GM coefficients, are expected to be statistically identical in the zonal direction. A meridionally-varying GM coefficient κ can be calculated using the time mean zonal mean of the thickness profiles and the thickness eddy fluxes through the formula

$$\kappa = -\frac{\overline{h'v'}}{\partial \bar{h} / \partial y}. \tag{12}$$

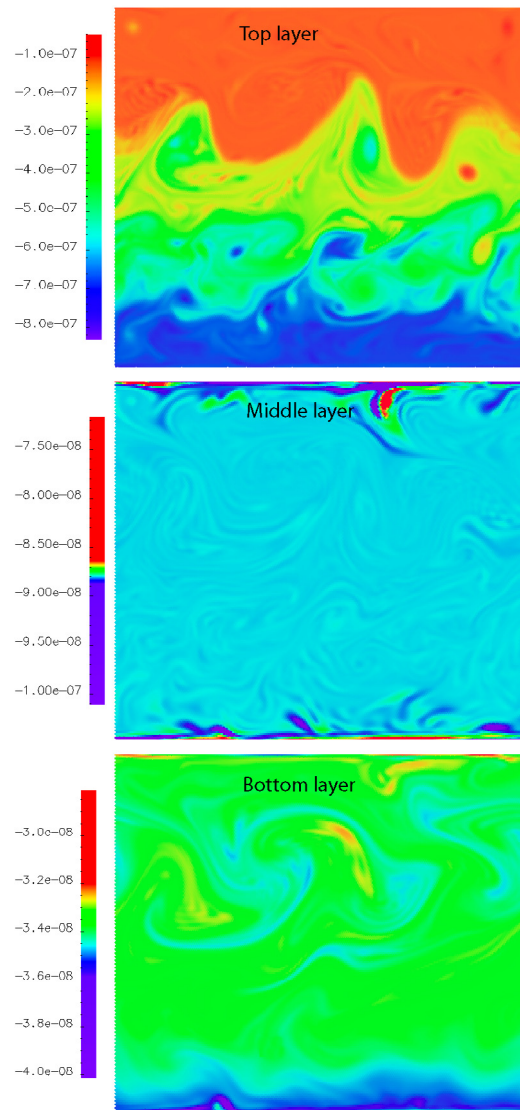


Fig. 1. Temporal mean of the potential vorticity for each layer around year 200. The colormaps for each plot are not the same. (For interpretation of the references to color in this figure legend, the reader is referred to the web version of this article.)

The thickness profiles in Fig. 3 are flat in certain places, in particular near the boundary in the top and bottom layers. In those places the quotient on the right-hand side of (12) becomes extremely large and κ is singular. To remove the singularities, we bound the thickness gradient $\partial \bar{h} / \partial y$ by a quarter of the average slope of the meridional thickness profile, for each layer. The resulting smooth eddy diffusivity κ , for each layer, is plotted in Fig. 4. The κ for the top and bottom layers are predominantly positive, corresponding to the downgradient thickness eddy fluxes in these layers. The values are within the range between 0 and 2000 m^2/s , consistent with results from the previous literature (e.g. [2]). The eddy diffusivity κ for the middle layer is positive on the pole side and negative on the equator side of the channel midpoint.

Results from low resolution simulations

Ringler and Gent [16] shows that the eGM closure is marginally better than the standard GM, when the eddy transport coefficient is assigned a constant 500 m^2/s and the eddy mixing coefficient (κ on the right-hand side of (9)) is assigned a smaller constant 250 m^2/s . The motivation for the reduced parameter value is the strong reverse jet flows seen in the case of eGM with a larger value 500 m^2/s for the eddy mixing coefficient. This work aims to test the hypothesis from [16] that this deficiency for eGM can be remedied by the use of spatially varying eddy diffusivities. The general model configurations are listed in Table 1. The two model configurations studied in this work are the standard GM (referred to as GM) and the extended GM (referred to as eGM). In GM, the large-scale thickness transport velocity \mathbf{u} is replaced by the effective transport velocity \mathbf{U} . In eGM, both the large-scale thickness transport velocity and the velocity component involved in the nonlinear

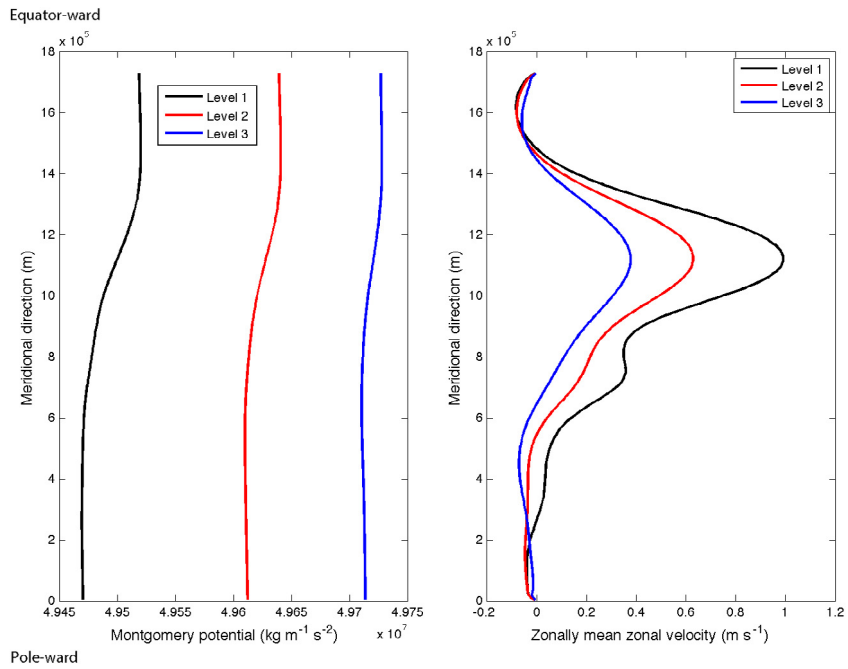


Fig. 2. Mean Montgomery potential and zonal velocity.

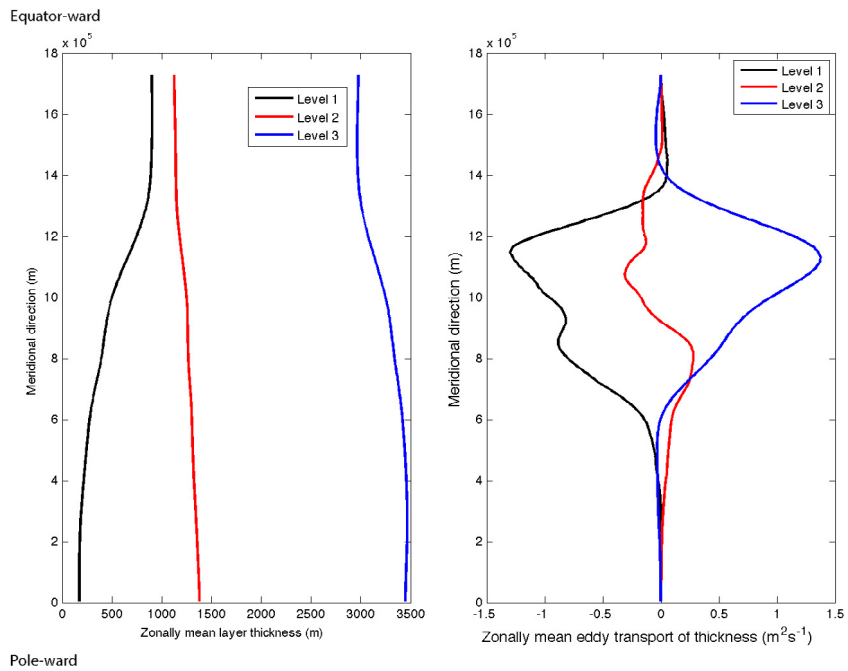


Fig. 3. Mean layer thickness (left) and meridional eddy thickness fluxes (right).

Coriolis forcing are replaced by the effective transport velocity \mathbf{U} . A PV mixing is also included on the right-hand side of the momentum equation (also see (9)).

The choices for the single parameter κ are listed in Table 2. The designation “const.” means that κ assumes a constant value $400 \text{ m}^2/\text{s}$, while “derived pos.” means that κ for the top and bottom layers are derived from the 10 km high-resolution reference simulations, with the negative numbers in them overwritten by zeros, and κ for the middle layer takes a constant $157 \text{ m}^2/\text{s}$, which is simply the average value of the eddy diffusivities in the middle layer. These designations will be used in the following discussion and in the figures.

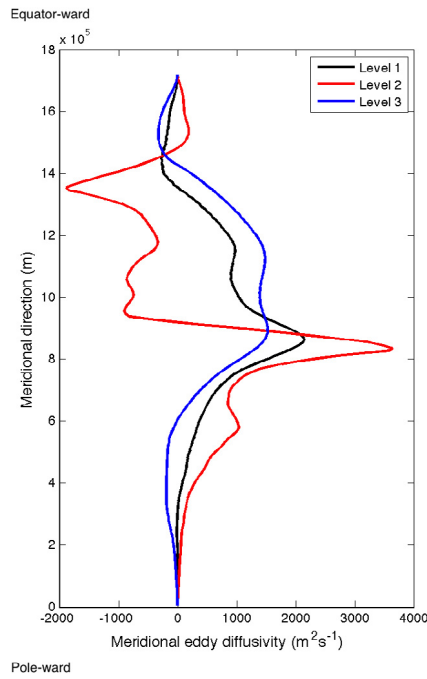


Fig. 4. Meridional eddy diffusivities derived from the mean meridional eddy thickness fluxes and the mean thickness profiles.

Table 1

Model configuration: equations. The transport velocity \mathbf{U} is the sum of the mean velocity \mathbf{u} and the bolus velocity \mathbf{u}^* , and \mathbf{u}^* is parameterized as $\mathbf{u}^* = -\kappa \nabla h/h$.

Designation	Thickness equation	Momentum equation
GM	$\frac{\partial h}{\partial t} + \nabla \cdot (h\mathbf{U}) = 0$	$\frac{\partial \mathbf{u}}{\partial t} + hq\mathbf{k} \times \mathbf{u} + \nabla(\phi + K) = 0$
eGM	$\frac{\partial h}{\partial t} + \nabla \cdot (h\mathbf{U}) = 0$	$\frac{\partial \mathbf{u}}{\partial t} + hq\mathbf{k} \times \mathbf{U} + \nabla(\phi + K') = \mathbf{k} \times (\kappa h \nabla q)$

Table 2

Model configuration: the parameters. The κ in eGM are determined in the same way.

Designation	Parameter determination
const.	$\kappa = 400 \text{ m}^2/\text{s}$ for all three layers
Derived pos.	κ for top and bottom layers are derived from 10 km high-res. simulations, with negatives overwritten by zeros; κ for the middle layer takes value $157 \text{ m}^2/\text{s}$.

For the low resolution simulations we use a 125 km uniform hexagonal grid so that mesoscale eddies are not resolved. The same numerical model based on MPAS is used, but with a biharmonic diffusion of $1.0 \times 10^{13} \text{ m}^4/\text{s}$ and with one of the configurations described above. We note that at this resolution, a biharmonic diffusion at the chosen level alone does not lead to stable simulations, but it is included in the simulations to facilitate the cascade of potential enstrophy. In evaluating the low resolution simulation results against the high resolution reference solutions, we choose the thickness, PV and zonal velocities for the initial comparisons. These variables are related to each, and together they provide a relatively complete picture of the channel flow.

Fig. 5 compares the time mean zonal mean thickness profiles of each low resolution simulation to those of the high resolution reference solutions. In the top layer, the thickness curves from the “GM derived pos.” and “eGM derived pos.” simulations are fairly close to that of the 10 km reference solution for most of the channel except near the northern boundary. In the bottom layer, clearly the thickness curve from the “eGM derived pos.” simulation is closest to that of the reference solution. The middle layer is challenging. The reference simulation maintains a sloped thickness curve to support a homogeneous PV field, whereas down-gradient GM parametrizations work to flatten the thickness curve. However, the thickness curves generated by both of the eGM simulations are largely consistent with that of the reference solution. The conclusions one can draw by comparing the time mean zonal mean PV profiles to those of the reference solution (see Fig. 6) agree with those we have just laid out when comparing the thickness profiles. This is a result of the PV field predominantly determined by the planetary vorticity and thickness fields. When evaluated as a whole, these comparisons show that the eGM model configuration, combined with the “derived pos.” parameters, produce the overall best results in terms of thickness and PV.

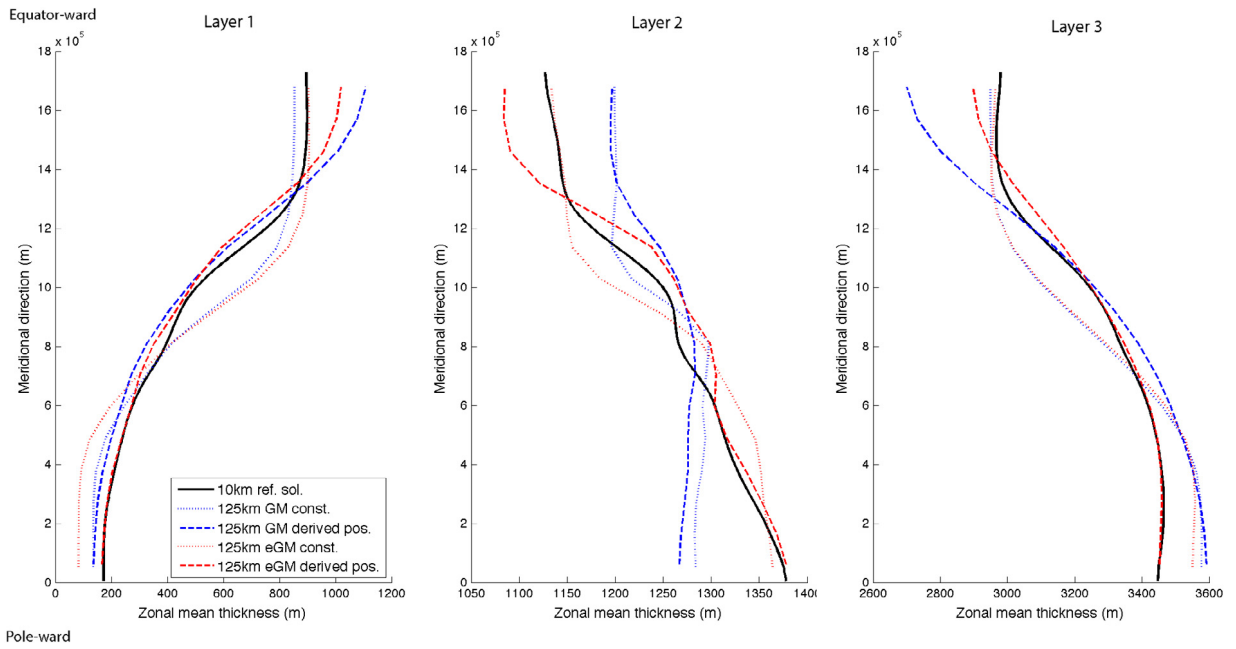


Fig. 5. Mean thickness for each layer from the reference solution and the various low resolution solutions.

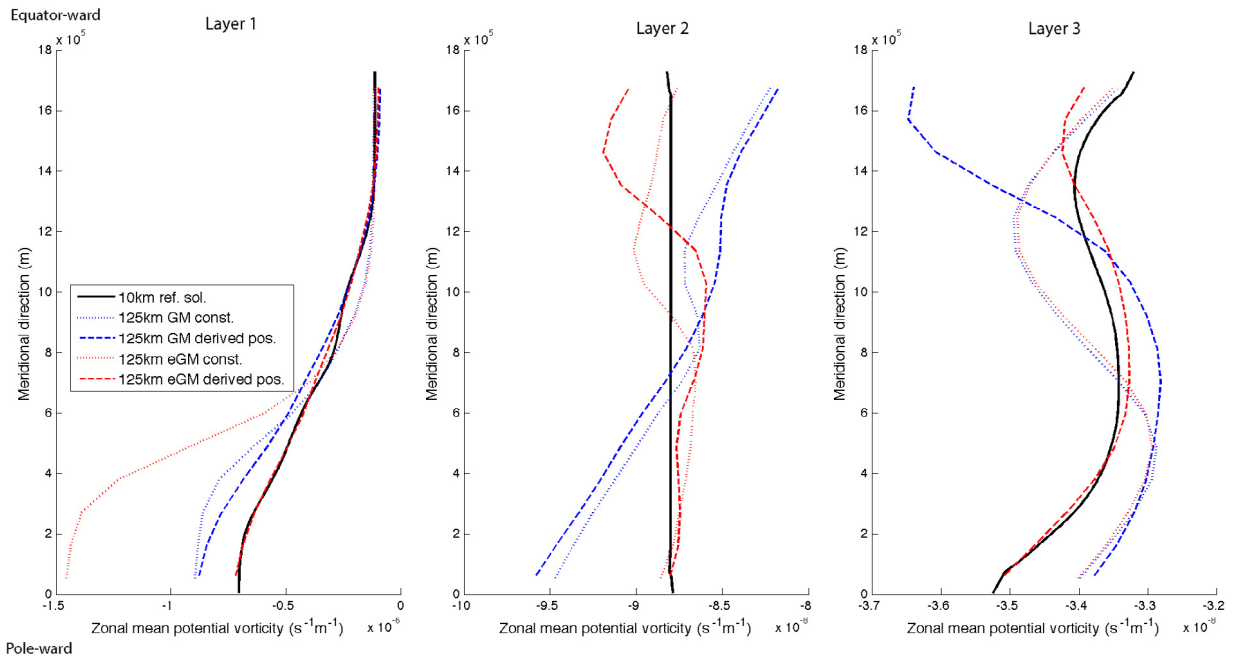


Fig. 6. Mean potential vorticity for each layer from the reference solution and the various low resolution solutions.

Fig. 6 also sheds lights on the impact of the PV gradient term in the momentum equation (11). The nearly y-independent PV curves generated by eGM with both types of coefficients in the middle layer show that the PV gradient term can effectively shut itself off in the interior of the flow, when no external forcing is present, resulting in states close to the reference solution. In the top layer, all the PV curves have a positive meridional gradient throughout the channel. For the low-resolution simulations, this means that the PV gradient on the RHS of Eq. (11) acts to slow down the jet, consistent with the role of the mesoscale eddies in that regime. In the jet region (from 600 to 1400 km), the slope of the PV curves for the eGM simulations is approximately $3 \times 10^{-13} \text{ m}^{-2} \text{ s}^{-1}$. With $\kappa = 400 \text{ m}^2 \text{ s}^{-1}$ and $h = 600 \text{ m}$ (both characteristic values of the jet region), the RHS of Eq. (11) is approximately $7.2 \times 10^{-8} \text{ m s}^{-2}$. In comparison, when the flow is at rest, the RHS of Eq. (11) is essentially $\kappa \beta$, and with the same value for κ it is approximately $5.6 \times 10^{-9} \text{ m s}^{-2}$. Hence, at equilibrium, the PV gradient term of Eq. (11)

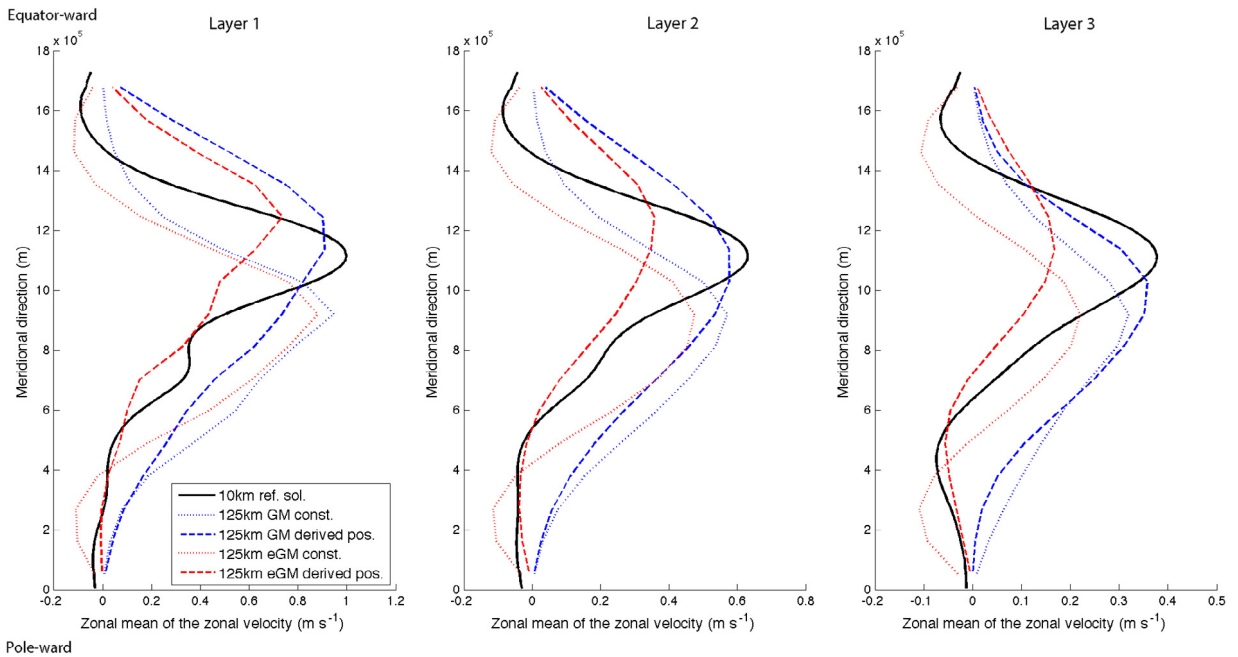


Fig. 7. Mean zonal velocity for each layer from the reference solution and the various low resolution solutions.

is amplified. The other leading terms in the equation are the Coriolis term $f\bar{v}_1$, which is approximately $2.8 \times 10^{-7} \text{ m s}^{-2}$ (with \bar{v}_1 about $2.5 \times 10^{-3} \text{ m s}^{-1}$ diagnosed from both high-resolution and low resolution simulations), and the external forcing $\tau_0/\rho h$, which is about $1.6 \times 10^{-7} \text{ m s}^{-2}$. Therefore, the PV gradient term of Eq. (11) is insignificant at rest compared to the external forcing, and at equilibrium, it amplifies and assists the Coriolis term to counterbalance the windstress.

The nearly y -independent PV in the middle layer means that a balancing gauge term in this layer, as suggested by Eden [15], would be very small. A balancing gauge term in the upper layer would be much larger, but would still be considerably smaller than the wind forcing and Coriolis terms. Therefore, we believe that the momentum non-conservation in these eGM solutions is not a large problem, and that solutions where a gauge term evaluated layer by layer is included would not be significantly different than those presented here.

Fig. 7 shows the time mean zonal mean of the zonal velocities for the low resolution and the high resolution simulations. Overall, for each layer the GM simulations, regardless of the choice of the GM parameters, are able to produce higher maximum velocities that are close to those of the reference solutions. But the jets generated by these low resolution simulations are much wider than those in the reference flow. The jets generated by the eGM simulations are slower, but with widths that are more comparable to those in the reference flow. The westward jets present near the boundaries in the eGM simulation with constant coefficients are removed in the simulation with derived positive coefficients. It is also worth noting that, across all three layers, the jets produced by eGM with constant coefficients lag behind those reference jets by about 0.16 m s^{-1} in terms of the maximum speeds, and the jets produced by eGM with derived positive coefficients lag behind by about 0.3 m s^{-1} , indicating that eGM is good at reproducing the baroclinic structures of the flow, and the differences between the low resolution solutions and the high resolution reference solution are largely barotropic.

The initial evaluation so far shows that eGM with the “derived pos.” parameters performs slightly better than the other model configurations, but it is not clear which configuration is best at reproducing the zonal velocities for the jets. We adopt two additional metrics for the evaluation. The first metric compares how well these model configurations reproduce the volume fluxes of the ACC, and the second metric compares how well these model configurations reproduce the thickness profiles in terms of L^2 norms. The first metric certainly has its physical relevance, and the second metric provides a quantitative measure of the performance of various model configurations in reproducing the isopycnal structures in the flow. These two metrics are complementary, because the volume fluxes are essentially determined by the end points of the isopycnal curves when the flow is in geostrophic balance, which has been shown to be the case (see Fig. 2), and the L^2 -norm measures the errors over the whole meridional span of the jet.

Fig. 8 compares the volume fluxes of each model configuration in all three layers to those of the reference solution. Unsurprisingly, the two GM simulations over-estimate the volume fluxes in all three layers. In the middle layer, they over-estimate the fluxes by over 67%, and by about 100% in the bottom layer. On the other hand, the two eGM simulations tend to under-estimate the volume fluxes except for the eGM model with derived positive parameters in the top layer where it slightly over-estimates the fluxes. This model configuration under-estimates the fluxes by about 13% in the middle layer and by about 42% in the bottom layer. In Fig. 9, we plot the global L^2 errors in the thickness profiles compared to the reference solutions. Among the four model configurations listed in Tables 1 and 2, the eGM model with derived positive parameters

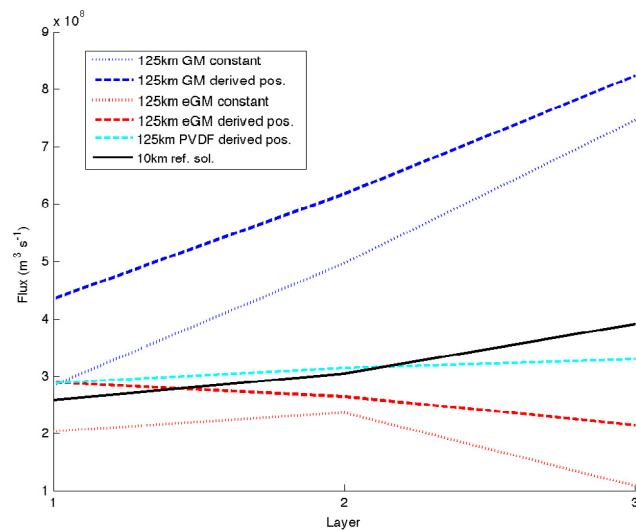


Fig. 8. Comparison of volume fluxes across a vertical-meridional cross-section.

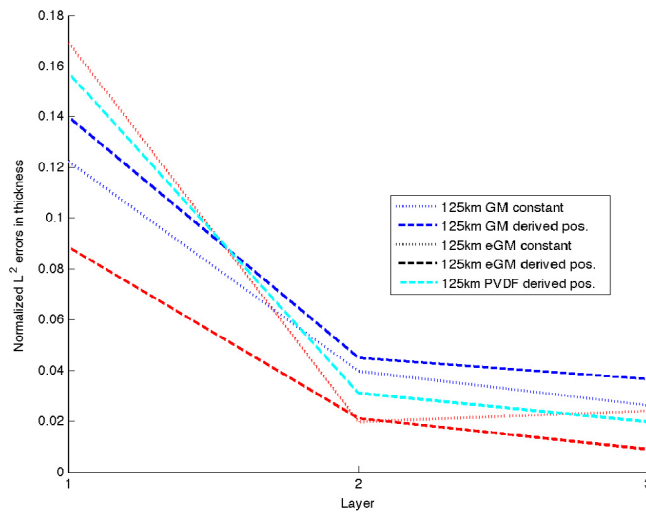


Fig. 9. Comparison of the L^2 errors in the mean thickness for each layer.

consistently has the smallest errors for all three layers. Both the volume-flux and the L^2 -error metrics suggest that the eGM model with derived positive parameters has the overall best performance.

The eGM momentum equation (9) contains two extra terms that are attributed to meso-scale eddies: the eddy PV transport on the left-hand side and the eddy PV mixing on the right-hand side. It is natural to ask which one of them contributes more to the improvement of the eGM model? The PV mixing on the right-hand side is necessary for stable simulations at this level of resolution. We are left with the option of turning off the parametrization of the eddy PV transport on the left-hand side. We call the resulting model PVDF. Compared to the eGM model with derived positive parameters, the PVDF model with the same choice of parameters produces the same amount of volume flux in the top layer, and increased volume fluxes in the middle and bottom layers (Fig. 8), which are also closer to those of the reference solutions. From this we deduce that, in the middle and bottom layers, the eddy PV transport has the effect of decelerating the jets. The same model configuration leads to a surge in the L^2 -errors in the thickness profiles for all three layers, which indicates that the eddy PV transport is essential in getting the improved thickness profiles.

In our study two additional parameter variations are used but their results are not reported here either because they are unacceptable or they are weaker than what we have presented. Nevertheless, we describe these variations here for the purpose of record. In one of the variations, κ assumes values from the 10 km high resolution reference simulation verbatim (see Fig. 4). In spite of the presence of negative values for the eddy diffusivity, the low resolution simulation is able to run to completion, but the system is very sensitive to small perturbations, and its final state is drastically different from the reference solution. In the other variation, κ assumes only positive values from the high resolution reference simulation;

κ takes zero where the eddy diffusivity is negative. The difference between this variation and the “derived pos.” option is in the middle layer: this variation assumes non-negative values from the high-resolution reference simulation while the “derived pos.” assumes a positive constant. The results from this variation are similar to those of “derived pos.” option, but are slightly worse in reproducing the PV profiles in the top and middle layers (plots not shown).

4. Concluding remarks

Through a set of controlled simulations with a three-layer isopycnal model for the ACC, this study confirms a hypothesis made in [16] that using spatially varying eddy diffusivities can remedy the deficiency of strong reverse jets near the channel boundaries for the extended GM closure. In this general setting, the study also demonstrates that the extended GM with eddy diffusivities derived from the high resolution reference simulation produces the best low resolution solution in terms of the thickness and PV profiles and the volume fluxes across all three vertical layers.

Data from the high-resolution reference simulation show that the eddy diffusivities are mostly positive in the top and bottom layers. This indicates that the eddy thickness fluxes are predominantly down the thickness gradients, consistent with the fundamental assumption of the GM parametrization for the mesoscale eddy transport. The data also show that the eddy diffusivities in the middle layer have mixed signs, contradicting the assumption of the GM closure. This suggests that, in the “non-ventilated” interior of the ocean, care has to be taken when applying the GM closure. In this study, we experiment with two options for the GM parameters in the middle layer, one with a small but positive constant and the other with non-negative values derived from the high-resolution reference solutions. Both options lead to a PV field in the middle layer that is like the planetary vorticity f and inconsistent with the theory of Rhines and Young [17]. An alternative approach could be to apply a different type of closure in the middle layer, e.g. [14].

The basic premise of eGM is that mesoscale eddies can be better parameterized by transporting and mixing PV in a fashion similar to tracers. This can be accomplished by (1) using the residual velocity rather than the mean velocity in the Coriolis force and (2) modifying the RHS dissipation to act on gradients of PV instead of vorticity. Both of these modifications are, in essence, altering the forces applied to the mean momentum equation. However, as discussed in [11,15], strict adherence to down-gradient PV mixing can violate conservation of momentum. The eGM closure used here is not free of this serious issue. But, the numerical results of this work demonstrate that the PV mixing term of eGM is self-adjusting and self-limiting in the sense that it is insignificant at rest, and at equilibrium it effectively shuts itself off in the interior of the flow, and amplifies in the top layer to help counter-balance the windstress. Therefore, we have chosen not to balance the non-conservation in the momentum equation because the PV mixing is not the dominant term in the top layer and is very small in the middle layer. Thus, balancing the momentum conservation layer by layer would make a relatively small change to the results presented in this paper. The recent analyses of Marshall et al. [21], Young [22] and Maddison and Marshall [23] demonstrate that the correct modification of the momentum equation is not by parameterizing the *forces* directly, but rather by parameterizing a *stress tensor* and applying its divergence to the momentum equation for the residual velocity. This method assures conservation of momentum, energy and a PV based on the residual velocity.

This study is part of a project to develop scale-aware mesoscale eddy parametrizations for use in the next-generation multi-resolution ocean models. Chen et al. [24,25] made the first step by developing and evaluating a scale-aware version of the anticipated potential vorticity method in the idealized shallow water setting. There, the two-dimensional isotropic turbulence theory is employed to derive a formulation for the coefficient for the Anticipated Potential Vorticity Method, which depends on a single scale-invariant parameter. Experiments on a suite of multi-resolution grids show that the new formulation is able to scale across the wide range of grid lengths existing on the grids and bring the potential enstrophy spectrum curves throughout the inertial range evenly close to that of the reference solution. The current study takes a step forward and evaluates the merits of spatially varying eddy diffusivities for the widely used GM closure in an isopycnal model for the ACC. In this general setting, our study clearly demonstrates that using spatially-varying GM coefficients leads to improvements in reproducing certain features such as thickness profiles and volume fluxes of the high-resolution simulation. In the current study, we take the most direct approach by deriving the eddy diffusivities from a high-resolution reference simulation, which we will not have the luxury of replicating in real ocean simulations. Hence it will be necessary to test some of the many formulations for the GM coefficient that depend on the state of the flow and the local grid scales, such as Green [26]; Stone [27]; Visbeck et al. [7], Treguier et al. [12] and Eden [28], but this is not attempted in this paper.

Acknowledgments

We thank the anonymous reviewers for their helpful comments. This work was partially supported by the U.S. Department of Energy Office of Science program for Scientific Discovery through Advanced Computing (SciDAC) through the project of Multiscale Methods for Accurate, Efficient, and Scale-Aware Models of the Earth System, and by a grant from the Simons Foundation (#319070 to Qingshan Chen). NCAR is supported by the National Science Foundation.

References

- [1] P.R. Gent, J.C. McWilliams, Isopycnal mixing in ocean circulation models, *J. Phys. Oceanogr.* 20 (1) (1990) 150–155.
- [2] P.R. Gent, J. Willebrand, T.J. McDougall, J.C. McWilliams, Parameterizing eddy-induced tracer transports in ocean circulation models, *J. Phys. Oceanogr.* 25 (4) (1995) 463–474.

- [3] P. Gent, The Gent–McWilliams parameterization: 20/20 hindsight, *Ocean Modell.* 39 (1–2) (2011) 2–9.
- [4] M.H. Redi, Oceanic isopycnal mixing by coordinate rotation, *J. Phys. Oceanogr.* 12 (10) (1982) 1154–1158.
- [5] G. Danabasoglu, J. McWilliams, P. Gent, The role of mesoscale tracer transports in the global ocean circulation, *Science* 264 (5162) (1994) 1123–1126.
- [6] G. Danabasoglu, J. McWilliams, Sensitivity of the global ocean circulation to parameterizations of mesoscale tracer transports, *J. Clim.* 8 (12) (1995) 2967–2987.
- [7] M. Visbeck, J. Marshall, T. Haine, M. Spall, Specification of eddy transfer coefficients in coarse-resolution ocean circulation models, *J. Phys. Oceanogr.* 27 (3) (1997) 381–402.
- [8] R. Farneti, P. Gent, The effects of the eddy-induced advection coefficient in a coarse-resolution coupled climate model, *Ocean Modell.* 39 (1–2) (2011) 135–145.
- [9] M. Hofmann, M.A. Morales Maqueda, The response of Southern Ocean eddies to increased midlatitude westerlies: A non-eddy resolving model study, *Geophys. Res. Lett.* 38 (3) (2011).
- [10] P. Welander, Lateral friction in the oceans as an effect of potential vorticity mixing, *Geophys. Fluid Dyn.* 5 (1) (1973) 173–189.
- [11] J.C. Marshall, On the parameterization of geostrophic eddies in the ocean, *J. Phys. Oceanogr.* 11 (2) (1981) 257–271.
- [12] A. Treguier, I. Held, V. Lariève, Parametrization of quasigeostrophic eddies in primitive equation ocean models, *J. Phys. Oceanogr.* 27 (1997) 567–580.
- [13] R. Greatbatch, Exploring the relationship between eddy-induced transport velocity, vertical momentum transfer, and the isopycnal flux of potential vorticity, *J. Phys. Oceanogr.* 28 (3) (1998) 422–432.
- [14] D.P. Marshall, R.G. Williams, M.-M. Lee, The relation between eddy-induced transport and isopycnal gradients of potential vorticity, *J. Phys. Oceanogr.* 29 (7) (1999) 1571–1578.
- [15] C. Eden, Parameterising meso-scale eddy momentum fluxes based on potential vorticity mixing and a gauge term, *Ocean Modell.* 32 (2010) 58–71.
- [16] T. Ringler, P. Gent, An eddy closure for potential vorticity, *Ocean Modell.* 39 (2011) 125–134.
- [17] P. Rhines, W. Young, Homogenization of potential vorticity in planetary gyres, *J. Fluid Mech.* 122 (1982) 347–367.
- [18] J. McWilliams, J. Chow, Equilibrium geostrophic turbulence. 1. A reference solution in a Beta-Plane channel, *J. Phys. Oceanogr.* 11 (7) (1981) 921–949.
- [19] T.D. Ringler, J. Thuburn, J.B. Klemm, W.C. Skamarock, A unified approach to energy conservation and potential vorticity dynamics for arbitrarily-structured C-grids, *J. Comput. Phys.* 229 (9) (2010) 3065–3090.
- [20] T. Ringler, M. Petersen, R.L. Higdon, D. Jacobsen, P.W. Jones, M. Maltrud, A multi-resolution approach to global ocean modeling, *Ocean Modell.* 69 (2013) 211–232.
- [21] D.P. Marshall, J.R. Maddison, P.S. Berloff, A framework for parameterizing eddy potential vorticity fluxes, *J. Phys. Oceanogr.* 42 (4) (2012) 539–557.
- [22] W.R. Young, An exact thickness-weighted average formulation of the Boussinesq equations, *J. Phys. Oceanogr.* 42 (2012) 692–707.
- [23] J.R. Maddison, D.P. Marshall, The Eliassen–Palm flux tensor, *J. Fluid Mech.* 729 (2013) 69–102.
- [24] Q. Chen, M. Gunzburger, T. Ringler, A scale-invariant formulation of the anticipated potential vorticity method, *Mon. Weather Rev.* 139 (8) (2011) 2614–2629.
- [25] Q. Chen, M. Gunzburger, T. Ringler, A scale-aware anticipated potential vorticity method. Part II: on variable-resolution meshes, *Mon. Weather Rev.* 140 (9) (2012) 3127–3133.
- [26] J.S.A. Green, Transfer properties of the large-scale eddies and the general circulation of the atmosphere, *Q. J. R. Meteorol. Soc.* 96 (408) (1970) 157–185.
- [27] P. Stone, A simplified radiative-dynamical model for the static stability of rotating atmospheres, *J. Atmospheric Sci.* 29 (3) (1972) 405–418.
- [28] C. Eden, A closure for meso-scale eddy fluxes based on linear instability theory, *Ocean Modell.* 39 (3–4) (2011) 362–369.